Effectiveness of Silicon (Si) as a Laser Shinethrough Barrier for 351-nm Light

Introduction

In direct-drive inertial confinement fusion (ICF), energy from many individual high-power laser beams is delivered to a spherical target, causing a spherically symmetric implosion.[1] Current ignition designs for direct-drive targets require a layer of condensed D_2 or DT fuel that adheres to the inner surface of a spherical plastic-shell ablator. The laser ionizes the target shell's surface, forming a plasma that surrounds the target. This coronal plasma governs any further interaction of the laser and the target, and the critical surface within the plasma prevents further direct transmission of light into the target's interior. The laser energy is absorbed in the subcritical underdense plasma and transported by the electrons through the overdense plasma to the ablation front. The ablation pressure drives the fuel layer inward, compressing both it and the gaseous fuel at the target's center. The drive pressure is varied in time such that the fuel density is compressed (up to ~1000× solid density for ignition designs) while remaining close to Fermi degenerate. Shock waves resulting from the drive-pressure history, along with compressive work, heat the central gaseous-core "hot spot" to the high temperatures needed to initiate burning of the fuel.

Asymmetry-induced hydrodynamics can reduce the performance of ICF targets to well below that predicted by 1-D modeling.[2] The hydrodynamic instability of most concern is Rayleigh–Taylor instability (RTI).[3,4] Imperfections in the spherical symmetry of both the target structure and the laser illumination act as seeds for the RTI. The nonlinear growth of this instability on the inner surface of the target mixes the cold compressed fuel layer with the hot-spot fuel vapor and/or shell, reducing fusion yield or preventing ignition.[5–8] Ignition requirements impose severe constraints on the illumination uniformity and the sphericity of the target.[9]

It has long been known[10,11] that very early during laser irradiation, before the coronal plasma density reaches critical density, the target is transparent to the laser light and laser energy can penetrate into the target. Deposition of this laser "shinethrough" energy within the target can severely degrade target performance even though the total energy is small. Absorption of shinethrough laser light can transmit nonuniformities in the illumination due to power imbalance or imprint into the target's interior. These asymmetries are made worse by filamentation of the penetrating laser power inside the target, which has been observed to leave permanent damage tracks.[10] The nonuniform deposition of energy in the interior of the target can create density perturbations that seed the RTI.

Shinethrough-seeded RTI has been identified as the likely cause of anomalous results in "burnthrough" mass-ablation-rate experiments.[12,13] In these experiments, a high-Z tracer layer was embedded within a target as a diagnostic, and the onset time of characteristic x-ray radiation from that layer during an implosion was used to infer the burnthrough ablation rates. The measured ablation rates were far greater than predicted by 1-D modeling. The spatial distribution of the characteristic x rays was found to be emitted from many localized spots.[13] The addition of an opaque barrier layer on the target surface was shown to bring the characteristic x-ray onset time in line with the 1-D predictions.[12]

A thin barrier layer of UV opaque material on the outer surface of the target forces breakdown to occur at the outer surface, effectively eliminating the deleterious effects of shinethrough. The conventional material used for shinethrough barriers is aluminum (Al). Barrier layers of Al have been shown to block shinethrough light and improve implosion performance. A thin barrier layer of 200 Å of Al eliminated all signs of filamentation damage tracks in laser-illuminated targets.[10] Deuterium-filled glass targets with a 500-Å Al barrier imploded using the original 24-beam OMEGA Laser System[14] showed a clear yield improvement over uncoated targets.[11]

For direct-drive cryogenic targets on OMEGA, a suitable shinethrough barrier material must be opaque to the 351-nm UV laser light *and* be compatible with the standard cryogenic target fabrication techniques of permeation filling, infrared (IR) layering, and optical characterization. The common Al barrier material is unsuitable in this context in all respects. In

the past, silicon (Si) has been identified as a potential barrier material for cryogenic direct-drive targets.[15] Its transmission characteristics are sufficient for optical characterization at 627 nm (Fig. 115.35) and laser-assisted cryogenic layering at 3.16 μm, and it is suitable for permeation filling.

At the laser wavelength (351 nm) the Si barrier is almost opaque and its opacity increases with laser intensity due to the easy formation of free electrons in Si. Silicon thus appears to be an excellent candidate for a shinethrough barrier material.
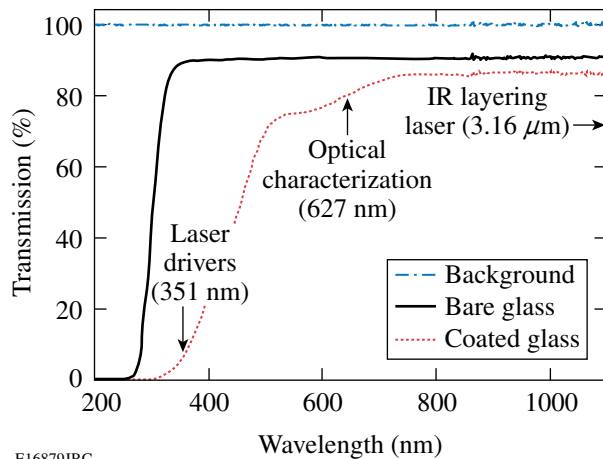
Figure 115.35
Transmission of light through uncoated glass and through glass coated with ~1100 Å of Si. The silicon-coating transmission is low at the UV laser driver wavelength (351 nm) and high at the ice-layer optical characterization wavelength (627 nm).

In this article we experimentally verify the suitability of Si as a shinethrough barrier material for 351-nm direct-drive laser-fusion experiments. The following sections (1) report the successful permeation filling, IR layering, and optical characterization of Si barrier–coated cryogenic targets; (2) experimentally verify the performance of Si as a shinethrough barrier; (3) determine a minimum acceptable barrier thickness; and (4) discuss our conclusions.

Cryogenic Target Fabrication with Si Barriers

Cryogenic targets for OMEGA are permeation filled with either D_2 or DT at room temperature at approximately 1000 atm in the Fill/Transfer Station (FTS).[16] The targets are deuterated polystyrene shells of 3- to 10-μm wall thickness suspended in a beryllium "C-mount" using four submicron threads of spider silk. Once filled, the targets are cooled slowly (~0.1 K/min) to below their fuel triple point, forming rough ice layers inside the targets.[16]

The rough ice layers are subsequently smoothed using volumetric heating just below the triple point, which leads to a sublimation/condensation redistribution of the ice mass toward an inner surface that is smoother, more uniform, and closer to an isotherm. Volumetric heating naturally occurs in DT and T_2 fuels that self-heat due to tritium beta decay.[17,18] For D_2 fuel, the infrared heating technique[19] deposits energy volumetrically in the ice by pumping an IR collisionally induced vibration–rotation band of deuterium. The wavelength of the IR heating laser employed at LLE is 3.16 μm.

LLE uses optical backlit shadowgraphy to characterize OMEGA cryogenic target ice layers.[20,21] A 627-nm, red-light–emitting diode (LED) provides the backlighting. A shadowgram records the image of the light rays passing through a backlit target. The rays are reflected and refracted at the shell wall and ice-layer surfaces, forming characteristic rings in the shadowgram. The most-prominent ring or "bright ring" results from a single internal reflection off the inner solid/vapor interface of the ice layer. The position of the bright ring in the shadowgram is directly correlated with the position of the inner surface of the ice layer and makes it possible to characterize the nonuniformity of the inner surface. A 3-D reconstruction of the inner ice surface can be built from multiple shadowgrams from different views. Details can be found in Refs. 20 and 21.

To test the suitability of Si as a shinethrough barrier material, standard cryogenic target shells were coated with Si, then permeation filled, layered, and characterized using the standard procedures. Several typical OMEGA cryogenic shells were coated with Si using a room-temperature radio-frequency sputter coater. The Si thickness was estimated by a quartz crystal monitor, and the coating thickness was verified offline using reflected-light interferometry. The shells were affixed to a substrate with a weak adhesive and coated from above. The targets were flipped over at midpoint in the coating process to expose the other side. This single "roll-over" method produced some low-mode nonuniformity in the coating thickness, but the coverage was sufficiently uniform to test permeation filling, IR layering, or optical characterization of the Si-coated cryogenic targets. If Si barriers become common for spherical direct-drive targets, they will require a more-uniform coating technique than the roll-over method used here.

The optical shadowgrams of two Si barrier–coated cryogenic targets shown in Fig. 115.36 are proof that permeation filling and optical characterization through a Si barrier are possible. The shells, one coated with 500 Å of Si and the other with 1000 Å, were cooled to below the triple point for D_2

(18.73 K). Sufficient IR heating laser power kept the liquid layer in Fig. 115.36 from freezing. The shadowgrams in Fig. 115.36 show that both targets could be optically characterized.

A shadowgram and intensity lineout showing the ice layer of a DT permeation-filled target coated with 750 Å of Si are displayed in Fig. 115.37. The bright ring is very strong and two of the fainter inner rings are also clearly visible. A Fourier-mode power spectrum for the bright ring is shown in Fig. 115.38. The Si barrier did not significantly affect optical characterization
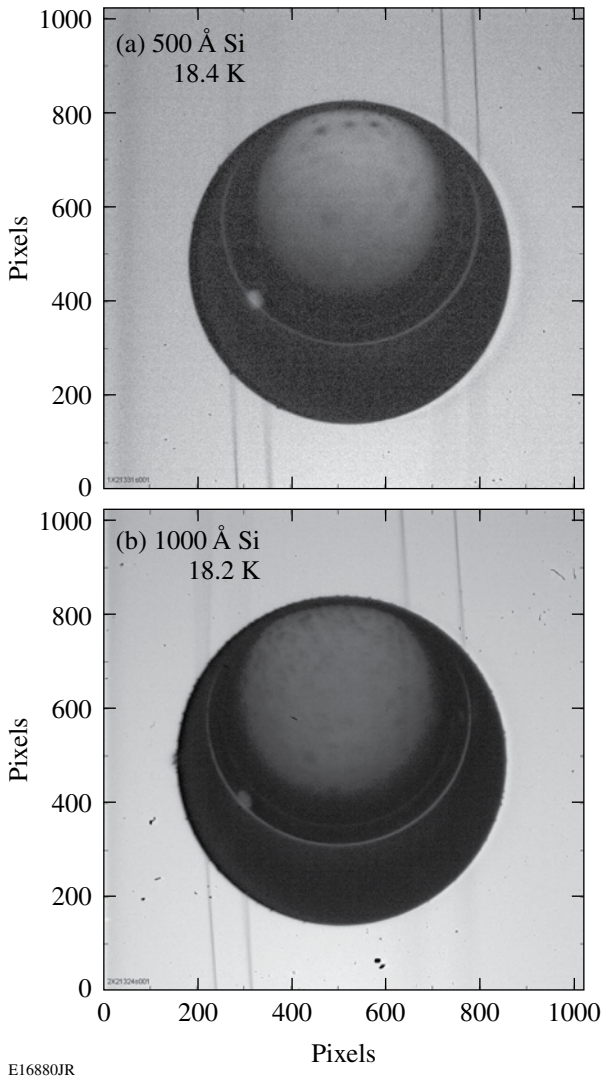
Figure 115.36

Backlit shadowgrams of permeation-filled cryogenic deuterium targets with Si shinethrough barrier coatings of (a) 500-Å and (b) 1000-Å thickness. The layering sphere temperatures are below the D_2 triple point, yet the fuel is still liquid. The off-center circular rings inside the target are the result of light internally reflecting off the vapor/liquid interface of the "bubble" inside the target.
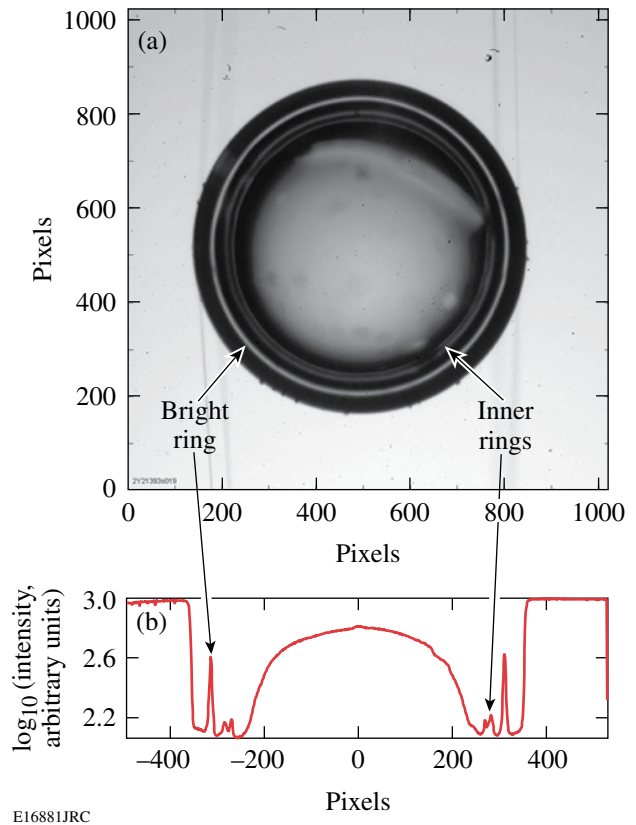

Figure 115.37

(a) Shadowgram of a Si-coated (750 Å), DT-filled cryogenic target and (b) a horizontal lineout through the target of the logarithm of the shadowgram intensity. Both the bright ring and two fainter inner rings are clearly visible through the Si barrier.
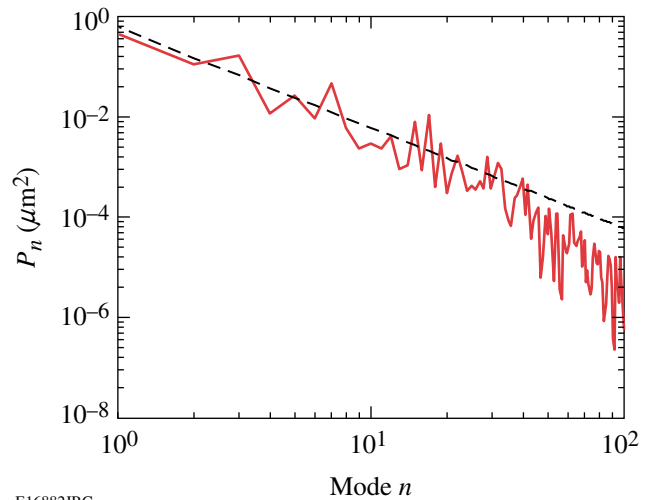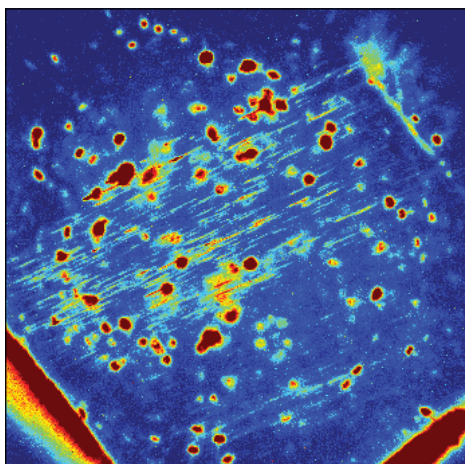

Figure 115.38

The Fourier-mode power spectrum of the bright ring (solid line) from Fig. 115.37 compared to the specification for direct-drive–ignition targets (dashed line).[9] The ice-surface rms for this view is 0.94 μm for all modes and for mode numbers 10 and above. This view is within the specification.

nor did the Si barrier inhibit beta layering of DT cryogenic targets. The surface-averaged rms (root mean square) of the ice-layer thickness for the target shown in Fig. 115.37 was 0.91 μm, one of the best layers produced to date for OMEGA.

The IR-layered, Si-coated D_2 cryogenic targets do not meet ignition specifications. Both targets shown in Fig. 115.36 showed large asymmetries when frozen with surface-averaged ice-layer-thickness nonuniformities of 6.2 μm (rms) for a 500-Å coating of Si and 11.6 μm (rms) for a 1000-Å coating of Si. While IR-layered D_2 targets typically have larger ice-layer asymmetries than DT targets, these values are among the worst in recent years and the target with the thickest Si barrier was more asymmetric. Determining whether these poor D_2 layers were statistical aberrations or were directly related to the Si coating will require further investigation.

Effectiveness of Si as a Shinethrough Barrier

Planar-target experiments were performed to verify the efficacy of Si and to determine the minimum effective thickness of Si as a shinethrough barrier material. Previous studies[11] have shown that the amount of shinethrough energy transmitted by an uncoated glass surface before a critical plasma forms is very low and is very insensitive to the incident laser intensity. The experiments were performed using a single beam at low energy (<1.5 J). The targets survived the experiments and clearly exhibited permanent shinethrough damage where there was no shinethrough barrier. Figure 115.39 shows filamentation damage streaks along the laser beam path behind an uncoated


E16883JRC

Figure 115.39
Post-shot close-up image of a glass-cube target ($4 \times 4 \times 4$ mm^3) showing filamentation tracks along the laser beam path through the target behind an uncoated region.

region of a glass target after exposure to a low-energy pulse (200 ps, 1.5 J).

The target in this experiment was a 6-mm $\times$ 6-mm $\times$ 1-mm glass slide constructed as detailed in Fig. 115.40(a). The target front was illuminated by a laser pulse of 200-ps duration and 0.7 J of energy. An examination of the target shows a distinctive "hourglass" hole burnt into the Al coating on the back of the target corresponding to the uncoated regions on the front of the target exposed to the beam. The Al backing is intact behind both the Al and Si shinethrough barrier squares on the front of the target. This is qualitative evidence that Si was as effective at blocking shinethrough as the conventional Al barriers.

A series of experiments using VISAR (velocity interferometry system for any reflector)[22,23] tested the efficacy of Si as a shinethrough barrier during a pulse. VISAR detects a Doppler shift of a probe beam reflected off a moving surface. The interference between two paths of the probe laser, one reflected off a surface and one direct to the detector, produces fringes whose displacements are proportional to the velocity of the surface. The effect of shinethrough light on an opaque surface can be detected using VISAR. Any shinethrough energy will heat the opaque layer, causing it to expand and resulting in movement of the VISAR fringes. If the heating is sufficient to vaporize the layer, the expanding material will disrupt the VISAR fringes and blank out this fringe pattern.

For these studies, the rear surfaces of several planar glass targets were covered with 1000 Å of Al to provide a reflective surface suitable for observation by VISAR. Half of the front (laser-facing) side was coated with a Si barrier. The low-power laser beam was centered on the interface between the Si-coated and uncoated portions of the target. The VISAR probe beam was pointed at the rear of the target to sample a line across the coated/uncoated interface. The results are summarized in Fig. 115.41. The VISAR fringes behind unprotected regions are blanked out promptly at the start of the illumination pulse, indicating an ablation of the rear surface by shinethrough energy. Note that in Fig. 115.41(b) this blanking is not seen because VISAR is observed behind only the Si barrier–protected region due to error in VISAR pointing, target alignment, or target metrology. The correct timing of the VISAR image with the laser pulse has been verified using the laser timing fiducial pulses (the dots visible along the top and bottom of each VISAR image). The VISAR fringes behind portions of the targets protected by 750-Å, 300-Å, and 200-Å Si barriers [Figs. 115.41(a)–115.41(c)] are unaffected by shinethrough, indicating no detectable motion or heating of the rear surfaces
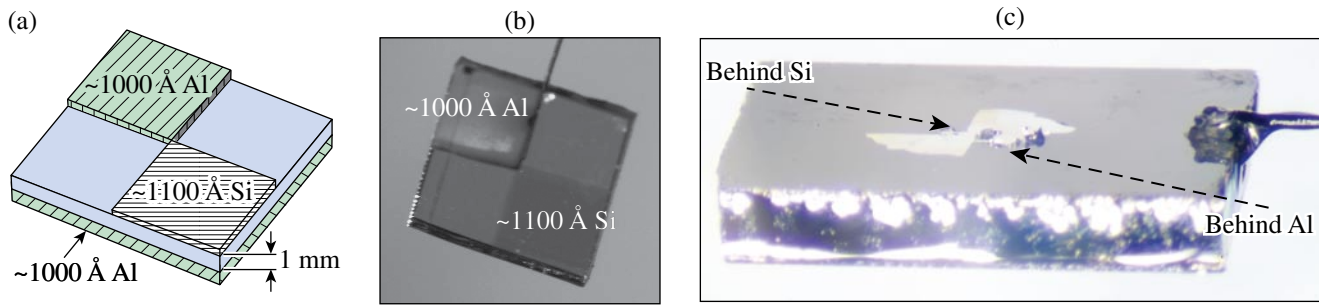
E16884JRC

Figure 115.40
Glass-slide planar target of dimensions roughly $6 \times 6 \times 1$ mm^3. (a) Design specifications: The back side of the target was coated with 1000 Å of Al. The front (laser-facing) side of the target was 1/4 coated with 1000 Å of Al, 1/4 coated with 1100 Å of Si, and 1/2 uncoated. (b) Pre-shot photograph of target front. (c) Post-shot photograph of back of target.
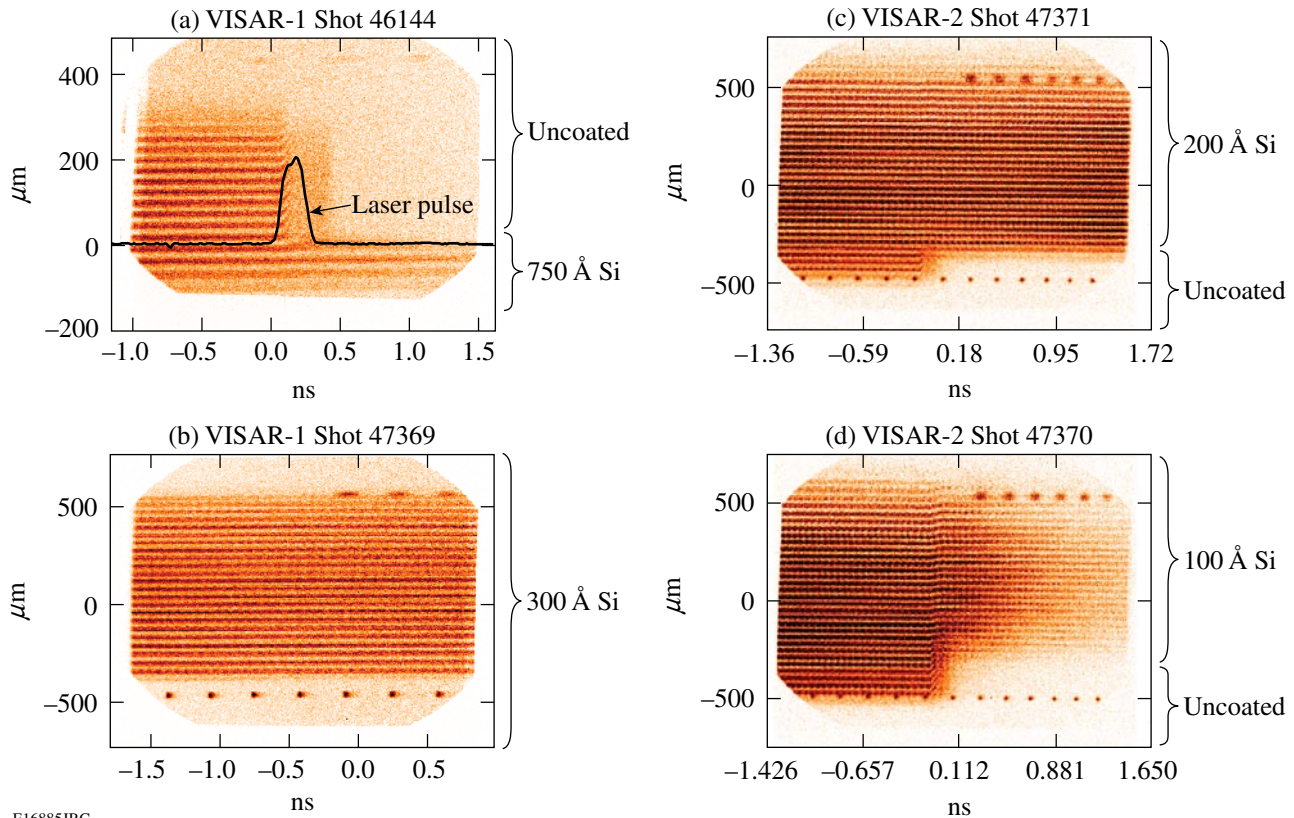
E16885JRC

Figure 115.41
VISAR fringes for four targets half coated with different thicknesses of Si: (a) 750 Å of Si, (b) 300 Å of Si, (c) 200 Å of Si, and (d) 100 Å of Si. The back surface behind the uncoated front is clearly ablated off by shinethrough at the start of the laser pulse [shown, for example, in (a) by the black line], blanking the VISAR signal wherever these unprotected sections are observed. The sections of the target protected by Si are unaffected except for the thinnest barrier layer in (d), where there is evidence of fringe motion behind the Si barrier–protected region, indicating motion/heating of the rear surface.

behind these barriers. Because the damage-threshold fluence for CH plastic is twice that for Al (Ref. 24), we conclude that these barrier thicknesses would have prevented shinethrough damage to an ICF plastic-shell target. In Fig. 115.41(d), however, the VISAR fringes show a slight motion of the surface behind a 100-Å Si barrier at the start of the pulse, clearly proving that some shinethrough energy has penetrated the Si barrier. From this VISAR data we conclude that a 100-Å Si coating is inadequate as a shinethrough barrier. A barrier layer of 200 Å of Si should be sufficient to block shinethrough light for 351-nm-laser–driven, direct-drive ICF plastic-shell targets. As previous studies[11] have shown that the total shinethrough energy transmitted before a critical surface forms in the coronal plasma is insensitive to the incident energy or intensity, this thickness should not need to be scaled for other experimental conditions. A 200-Å Si barrier should be sufficient to block shinethrough energy during the earliest part of the laser pulse before the coronal plasma reaches critical density in ICF and ignition experiments.

Discussion

These experiments have shown that direct-drive ICF cryogenic targets coated with up to 1000 Å of Si as a shinethrough barrier can be successfully permeation filled, beta-layered, and characterized. However, to minimize the effects of the barrier on these processes (such as the attenuation of light used to characterize the ice layer), we recommend using the minimum effective shinethrough barrier thickness of 200 Å of Si. This minimum thickness may also alleviate the possible difficulties with IR layering D_2 targets found in this study's limited sample set.

REFERENCES

1. J. Nuckolls *et al.*, Nature **239**, 139 (1972).

2. D. D. Meyerhofer, J. A. Delettrez, R. Epstein, V. Yu. Glebov, V. N. Goncharov, R. L. Keck, R. L. McCrory, P. W. McKenty, F. J. Marshall, P. B. Radha, S. P. Regan, S. Roberts, W. Seka, S. Skupsky, V. A. Smalyuk, C. Sorce, C. Stoeckl, J. M. Soures, R. P. J. Town, B. Yaakobi, J. D. Zuegel, J. Frenje, C. K. Li, R. D. Petrasso, D. G. Hicks, F. H. Séguin, K. Fletcher, S. Padalino, C. Freeman, N. Izumi, R. Lerche, T. W. Phillips, and T. C. Sangster, Phys. Plasmas **8**, 2251 (2001).

3. Lord Rayleigh, Proc. London Math Soc. **XIV**, 170 (1883).

4. G. Taylor, Proc. R. Soc. London Ser. A **201**, 192 (1950)

5. V. Lobatchev and R. Betti, Phys. Rev. Lett. **85**, 4522 (2000).

6. M. C. Herrmann, M. Tabak, and J. D. Lindl, Phys. Plasmas **8**, 2296 (2001).

7. R. Betti, K. Anderson, V. N. Goncharov, R. L. McCrory, D. D. Meyerhofer, S. Skupsky, and R. P. J. Town, Phys. Plasmas **9**, 2277 (2002).

8. R. P. J. Town and A. R. Bell, Phys. Rev. Lett. **67**, 1863 (1991).

9. P. W. McKenty, V. N. Goncharov, R. P. J. Town, S. Skupsky, R. Betti, and R. L. McCrory, Phys. Plasmas **8**, 2315 (2001).

10. J. E. Balmer, T. P. Donaldson, W. Seka, and J. A. Zimmermann, Opt. Commun. **24**, 109 (1978).

11. D. K. Bradley, T. Boehly, D. L. Brown, J. Delettrez, W. Seka, and D. Smith, in *Laser Interaction and Related Plasma Phenomena*, edited by H. Hora and G. Miley (Plenum Press, New York, 1991), Vol. 9, pp. 323–334.

12. J. Delettrez, D. K. Bradley, P. A. Jaanimagi, and C. P. Verdon, Phys. Rev. A **41**, 5583 (1990).

13. M. Nishikino *et al.*, Bull. Am. Phys. Soc. **46**, 142 (2001).

14. J. M. Soures, J. Fusion Energy **10**, 295 (1991).

15. Y. Fisher, T. R. Boehly, D. K. Bradley, D. R. Harding, D. D. Meyerhofer, and M. D. Wittman, Bull. Am. Phys. Soc. **43**, 1784 (1998).

16. D. R. Harding, T. C. Sangster, D. D. Meyerhofer, P. W. McKenty, L. D. Lund, L. Elasky, M. D. Wittman, W. Seka, S. J. Loucks, R. Janezic, T. H. Hinterman, D. H. Edgell, D. Jacobs-Perkins, and R. Q. Gram, Fusion Sci. Technol. **48**, 1299 (2005).

17. J. K. Hoffer and L. R. Foreman, Phys. Rev. Lett. **60**, 1310 (1988).

18. A. J. Martin, R. J. Simms, and R. B. Jacobs, J. Vac. Sci. Technol. A **6**, 1885 (1988).

19. D. N. Bittner *et al.*, Fusion Technol. **35**, 244 (1999).

20. D. H. Edgell, W. Seka, R. S. Craxton, L. M. Elasky, D. R. Harding, R. L. Keck, and M. D. Wittman, Fusion Sci. Technol. **49**, 616 (2006).

21. D. H. Edgell, R. S. Craxton, L. M. Elasky, D. R. Harding, S. J. Verbridge, M. D. Wittman, and W. Seka, Fusion Sci. Technol. **51**, 717 (2007).

22. L. M. Barker and R. E. Hollenbach, J. Appl. Phys. **43**, 4669 (1972).

23. P. M. Celliers, D. K. Bradley, G. W. Collins, D. G. Hicks, T. R. Boehly, and W. J. Armstrong, Rev. Sci. Instrum. **75**, 4916 (2004).

24. T. R. Boehly, Y. Fisher, D. D. Meyerhofer, W. Seka, J. M. Soures, and D. K. Bradley, Phys. Plasmas **8**, 231 (2001).